MATHEMATICAL MODELING AND COMPUTING, Vol. 9, No. 3, pp. 483–500 (2022)

A coupled compressible two-phase flow with the biological dynamics modeling the anaerobic biodegradation process of waste in a landfill

Belhachmi Z.[1,2], Mghazli Z.[3], Ouchtout S.[1,3]

[1] *University of Haute-Alsace, IRIMAS UR 7499, F-68100 Mulhouse, France*
[2] *University of Strasbourg, France*
[3] *Ibn Tofaïl University, Equipe d'Ingénierie Mathématique (EIMA), Laboratory: EDP, Algèbre et Géométrie Spectrale, B.P. 133, Kénitra, Morocco*

(Received 3 November 2021; Accepted 23 March 2022)

In this article, we present and study a new coupled model combining the biological and the mechanical aspects describing respectively the process of the biogas production and the compressible two-phase leachate-biogas flow during the anaerobic biodegradation of organic matters in a landfill, which is considered a reactive porous medium. The model obtained is governed by a reaction-diffusion system for the bacterial activity coupled with a compressible two-phase flow system of a non-homogeneous porous medium. We carry out the analysis and the numerical approximation of the model within a variational framework. We propose a full discrete system based on a second-order BDF-time scheme and P1-conforming finite element and we derive an efficient algorithm for the coupled system. We perform some numerical simulations in 2D and 3D examples in agreement with the theoretical analysis.

Keywords: *anaerobic biodegradation, compressible two-phase flow, biogas production, coupled model, finite element method.*

2010 MSC: 76M10, 76T10, 76-10, 92-10, 76V05 **DOI:** 10.23939/mmc2022.03.483

1. Introduction

Waste management and renewable energy generation are two key issues in nowadays society. A major research field arising in recent years focuses on combining the two topics mentioned above by developing new techniques to handle waste and use it in energy production. The anaerobic digestion process is a natural biological process of decomposing organic matter by microorganisms (bacteria) activated in the absence of oxygen. It consists of complex chemical reactions. In the long term, organic matter is transformed into "biogas", a mixture of methane and carbon dioxide. The main steps of the degradation process are hydrolysis, acidogenesis, acetogenesis and methanogenesis, described in bio-mechanical models by coupling the PDE and ODE systems (see [1–9]). Most of these models are too complex, widely empirical, and not well suited for mathematical analysis and computations. Increasing research activity has emerged in the modeling to obtain accurate results in waste management. We refer interested readers to [5, 10–16] and the references therein.

A bacterial dynamics model proposed by Bernard et al. [17], introduces a mere two-step process that singles out the dominant part in the bio-chemical transformations, namely the acidogenesis, using Monod's kinetics, and the methanogenesis using Haldane's kinetics. This approach is now very popular in the field and constitutes our starting point in this paper (e.g. see [1, 2, 18–22]).

Besides, the household waste landfill is a multi-phase medium consisting of solid, liquid, and gas and is considered to be a non-homogeneous reactive porous medium. The mechanical and biological dynamics are modeled by a coupled PDE-ODEs system describing the biodegradation process that produces biogas and leachate (see [23, 24] and the references therein). This approach is widely followed in the field, particularly for the control and the optimization of the biogas production purposes. However, it has some limitations, mainly due to the omission of the non-homogeneous character of

the porous medium and of the spatial distribution of the biological activity. In addition, influencing factors for accurate modeling, such as the role of humidity in the landfill, are underrated within this approach.

In [1], the authors proposed a modification of the above approach to overcome partially such limitations by spatializing the biological activity, which is now governed by a diffusion PDEs system coupled to a single-phase flow (from Darcy's flow equations).

In this article, we extend this novel approach to a two-phase flow where the gaseous phase "biogas" is included in the model. The goal is to have a more accurate consideration of the mechanical aspects of the complex interaction between the medium and the biological activity in the landfill. The resulting mathematical model and its numerical approximation lead to computation codes in 2D and 3D which improve prediction tools and waste degradation management.

The article is organized as follows: in Section 2, we introduce the coupled system of equations that consists of a unified model for the complex biological and mechanical interactions in the landfill. Firstly, we consider the standard ODEs system which describes the hydrolysis/acidogenesis and methanogenesis for the biogas production, under two specific growth rates [25]. In the way of [1], we transform the ODEs into a reaction-diffusion system of PDEs to spatialize the bacterial dynamics and to take into account the non-homogeneous distribution of methanogenese bacteria, which is a more realistic approach in a waste collection sites [26–28]. Secondly, we give the full system governing the compressible two-phase leachate-biogas flow and the biodegradation.

We emphasise that the consideration of the spatial distribution acts as a regularization procedure for the initial ODEs system, for which we have established in [25] the existence of several (stable and unstable) equilibria.

In Section 3, we consider the semi-discrete problems obtained with a second-order time scheme (BDF2) for the reaction-diffusion part and the semi-implicit Euler scheme for the two-phase flow equations. Section 4 is devoted to the full discrete system based on a standard P_1-conforming finite elements method. In Section 5, we present several 2D and 3D numerical results obtained by our computation code which is realized under the open source software FreeFem++ [29].

2. A coupled mathematical model for the biological dynamics and the flow

2.1. The bacterial dynamics: an anaerobic digestion system in two-step

The anaerobic digestion is a biological process that mineralizes organic substrates in the absence of the oxygen. The organic material is then transformed by microorganisms to a mixture (biogas) of methane (CH_4) and carbon dioxide (CO_2) through complex reactions in parallel and/or in series. The modeling of this phenomena has been extensively studied over last years and several mathematical models describing this process exist in the literature, especially concerning renewable energy (see [5, 10,11,30–32] and the references therein). The biogas production is a final step in the complex anaerobic digestion process called the methanogenesis.

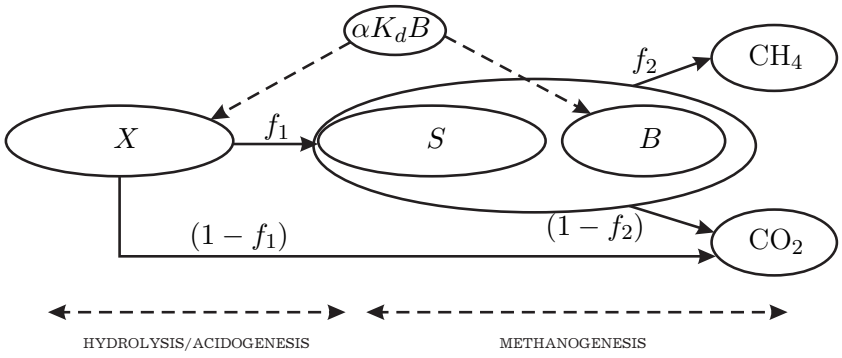

Fig. 1. Scheme used for modeling anaerobic degradation of organic mater.

The methane production process considered in this article is described as follows: a first step of hydrolysis/acidogenesis of the organic mater, represented by its concentration that we denote by X, leads to the formation of the carbon dioxide (CO_2) and a simple soluble organic mater S. The latter is used as a substrate by methanogenic bacteria B which in turn produce the carbon dioxide (CO_2) as well as the methane (CH_4). At their death, the methanogenic bacteria, in turn, constitute a complex substrate to hydrolysis step (see Fig. 1).

The parameters f_1 and f_2 are the stoichiometric coefficients which represent the parts of organic mater (OM) transformed into simple OM or methane during the "hydrolysis/acidogenesis" step or methanogenesis step, respectively. Consequently, $(1 - f_1)$ and $(1 - f_2)$ represent the parts of OM transformed into CO_2 during these two steps, respectively. K_d is the bacterial mortality rate and α is a constant $0 < \alpha \leqslant 1$ representing the fraction of the biomass mortality reused as a substrate in the methanogenesis. In what follows, we denote by K_h the rate of hydrolysis, Y the rate of use of the substrate and μ the specific growth rate.

Based on the principle of mass conservation and the law of bacterial growth, the model which describes the biological activity in this two-step process for biogas production is given firstly by the system of ordinary differential equations (1), and in which the existence of several (stable and unstable) equilibria has been established (see [25]),

$$\begin{cases} \dfrac{dX}{dt} = -K_h X + \alpha K_d B, \\ \dfrac{dB}{dt} = (\mu(S) - K_d)\, B, \\ \dfrac{dS}{dt} = f_1 K_h X - \dfrac{1}{Y}\mu(S)B, \\ \dfrac{d[\mathrm{CO_2}]}{dt} = (1 - f_1)K_h X + (1 - f_2)\dfrac{1 - Y}{Y}\mu(S)B, \\ \dfrac{d[\mathrm{CH_4}]}{dt} = f_2 \dfrac{1 - Y}{Y}\mu(S)B. \end{cases} \tag{1}$$

Next, we introduce the spatial diffusion (the spatial dependency of the bacterial dynamics), in order to consider the realistic case of nonhomogenous landfill, and to take into account some heterogeneities of the concentrations of microorganisms. This process was treated in the coupled model with the single phase leachate flow system (see [1]). We extend this novel approach to a two-phase flow where the gaseous phase, related to the biogas, is included in the model. The biodegradation model is then given as a reaction-diffusion system coupled with the flow system.

Let Ω be an open bounded subset of $\mathbb{R}^d$, $d \geqslant 2$, representing the landfill. We assume that its boundary $\Gamma := \partial\Omega$ is Lipschitz-continuous and is the union of two parts Γ_D and Γ_N, where Dirichlet and Neumann boundary conditions are respectively imposed, with $\Gamma_D \cap \Gamma_N = \varnothing$. The outward normal vector on Γ will be noted $\mathbf{n}$. We fix a time interval of biogas production $[0, T]$, where T corresponds to the moment when the leachate begins to stagnate at the bottom of the domain, or the moment when it is necessary to recover the biogas. Following the same approach as in [1], the biological activity can be modeled as follows:

$$(S1) \qquad \begin{cases} \dfrac{\partial \mathbf{U}}{\partial t} - \mathrm{div}\left(\bar{\bar{D}}\nabla \mathbf{U}\right) = \mathbf{F^1}(\mathbf{U}) & \text{in } \Omega\times]0,T[, \\ \dfrac{d\mathbf{G}}{dt} = \mathbf{F^2}(\mathbf{U}) & \text{in } \Omega\times]0,T[, \\ \bar{\bar{D}}\dfrac{\partial \mathbf{U}}{\partial n} = 0 & \text{on } \partial\Omega\times]0,T[, \\ \mathbf{U}(0,\cdot) = \mathbf{U}^0(\cdot), \quad \mathbf{G}(0,\cdot) = \mathbf{G}^0(\cdot) & \text{in } \Omega, \end{cases} \tag{2}$$

where $\mathbf{U}$ and $\mathbf{G}$ are the dynamic variables of the system (2) defined as follows

$$\mathbf{U} = (u_1, u_2, u_3)^t = (X, B, S)^t, \qquad \mathbf{G} = (u_4, u_5)^t = ([\mathrm{CO_2}], [\mathrm{CH_4}])^t \tag{3}$$

and $\bar{\bar{D}}$ is the diffusion coefficients matrix given as follows

$$\bar{\bar{D}} = \begin{pmatrix} D_1 & 0 & 0 \\ 0 & D_2 & 0 \\ 0 & 0 & D_3 \end{pmatrix},$$

where D_1, D_2 and D_3 are, respectively, the diffusion coefficients of X, B and S.

The right-hand terms $\mathbf{F^1}$ and $\mathbf{F^2}$ of the first and the second equations, respectively, in (2) are denoted by

$$\mathbf{F^1}(\mathbf{U}) = (F_1(U), F_2(U), F_3(U))^T, \quad \mathbf{F^2}(U) = (F_4(U), F_5(U))^T,$$

and the functions F_i, $i = 1, 2, \ldots, 5$ are defined as follows

$$\begin{aligned} F_1(\mathbf{U}) &= -K_h u_1 + \alpha K_d u_2, \qquad F_2(\mathbf{U}) = (\mu(u_3) - K_d)\, u_2, \\ F_3(\mathbf{U}) &= f_1 K_h u_1 - \frac{1}{Y}\mu(u_3)u_2, \quad F_5(\mathbf{U}) = f_2 \frac{1-Y}{Y}\mu(u_3)u_2, \\ F_4(\mathbf{U}) &= (1-f_1)K_h u_1 + (1-f_2)\frac{1-Y}{Y}\mu(u_3)u_2. \end{aligned}$$

Several laws exist for the specific growth rate $\mu(S)$. The most used are the Monod law

$$\mu(S) = \frac{\mu_m S}{K_S + S} \tag{4}$$

and the Haldane law

$$\mu(S) = \frac{\mu_m S}{K_S + S + \frac{S^2}{K_I}}, \tag{5}$$

where μ_m is the maximum growth rate, K_S is the half-saturation constant, and K_I is the inhibition constant. The Monod law is related to saturation and limitation phenomena and the Haldane law is related to saturation and inhibition phenomena [17]. We note that the Monod function can be considered as a particular case of the Haldane function for large values of the parameter K_I.

Remark 1. We remark that the second equation of (2) can be written as follows

$$\frac{d\mathbf{G}}{dt} = \mathbf{F^2}(\mathbf{U}) = \begin{bmatrix} (1-f_1)K_h u_1 + (1-f_2)\frac{1-Y}{Y}\left(\frac{du_2}{dt} + K_d u_2\right) \\ f_2 \frac{1-Y}{Y}\left(\frac{du_2}{dt} + K_d u_2\right) \end{bmatrix}.$$

This remark will be used in the Section 3.1 in order to linearize the system (2).

The system (2) allows us to compute the global rate of production of the biogas which constitutes the main part of the source/sink term in the next PDEs model of the flow in the waste.

2.2. Compressible two-phase leachate-biogas flow

The waste is considered as a porous medium consisting of a solid matrix, a liquid phase (leachate) and a gaseous phase formed by a binary mixture of methane and carbon dioxide (biogas). The modeling of a two-phase liquid-gas flow is based on a system of coupled equations (Darcy's law and the mass conservation equations) describing the flow of each phase simultaneously. In this context, we cite references [33–38] for a detailed description of these equations. Based on these references, we are interested in the two-phase leachate-biogas flow.

The mass conservation equation for each of the phases, biogas and leachate, are given by

$$\frac{\partial(\rho_b \theta_b)}{\partial t} + \operatorname{div}(\rho_b \mathbf{u}_b) = \alpha_b, \tag{6}$$

$$\frac{\partial(\rho_l \theta_l)}{\partial t} + \operatorname{div}(\rho_l \mathbf{u}_l) = \alpha_l. \tag{7}$$

Where $\mathbf{u}_i$, ρ_i and θ_i are respectively the velocity, the density and the volume content of the fluid $i = b, l$. The indices b and l represent the biogas and leachate phases respectively. α_l and α_b are the source term of leachate and the rate of the biogas generation respectively and which will be given later. In what follows, we denote by ϕ the porosity of the medium.

The flow velocity for each phase, leachate and biogas, is governed by the generalized Darcy's law (low Reynolds number $\mathrm{Re} < 1$):

$$\mathbf{u}_l = -K\frac{k_{rl}(\theta_l)}{\mu_l}(\nabla p_l - \rho_l g\,\mathbf{e_z}), \tag{8}$$

$$\mathbf{u}_b = -K\frac{k_{rb}(\theta_l)}{\mu_b}(\nabla p_b - \rho_b g\,\mathbf{e_z}). \tag{9}$$

where K, k_{rj}, p_j and μ_j are respectively the intrinsic permeability, the relative permeability, the pressure and the dynamic viscosity of phase j, for $j = l, b$. g is the modulus of the gravitational acceleration and $\mathbf{e_z} = \nabla z$ where z is the vertical axis directed downwards.

Source terms. The anaerobic digestion process needs water for the production of biogas, so the source term of leachate α_l is related to the rate of the biogas generation α_b. We follow the approach of [1, 17, 24, 32]:

$$\alpha_l = -\gamma\,\alpha_b = -\gamma\,\tilde{g}(\omega)\,A_m C_{Tb}\lambda_{cin},$$

where $\gamma = M_{\mathrm{H_2O}}/(3.4 \times M_b)$ with $M_{\mathrm{H_2O}}$ and M_b are respectively the molar mass of H_2O and the biogas, $\tilde{g}$ is an explicit function on the variable ω, the humidity rate defined by

$$\theta = \frac{\rho_0}{\rho}\omega$$

with ρ_0 the density of the dry medium, A_m is the biodegradable part of the waste, C_{Tb} is a positive constant and λ_{cin} is the rate of the biogas production (see [4] and [39]):

$$\lambda_{cin} = \frac{dC_{biogaz}}{dt} = \frac{d([\mathrm{CH_4}] + [\mathrm{CO_2}])}{dt}.$$

Experimental studies (see [32, 39]) show that below a minimal value ω_{min} and above a maximum value $\omega_{\max}$ there is no biogas production. The function $\tilde{g}$ increases in $[\omega_{\min}, \omega_1]$, is constant in $[\omega_1, \omega_2]$ and decreases in $[\omega_2, \omega_{\max}]$ for some values ω_1 and ω_2 (see Fig. 2).

The separation interface of the two fluids is characterized by an interfacial tension due to the effects of collision and adhesion between the two phases and so induces a pressure difference called capillary pressure:

$$p_c := p_b - p_l.$$

Capillary pressure and permeability depend on water content via different empirical models (see for example the models: Van Genuchten [40], Campbell [41] and Brooks–Corey [42]). We can find the parameter values of these model applied in biodegradation in the references [30–32]. We use here the Campbell model given as follows in the unsaturated porous medium case:

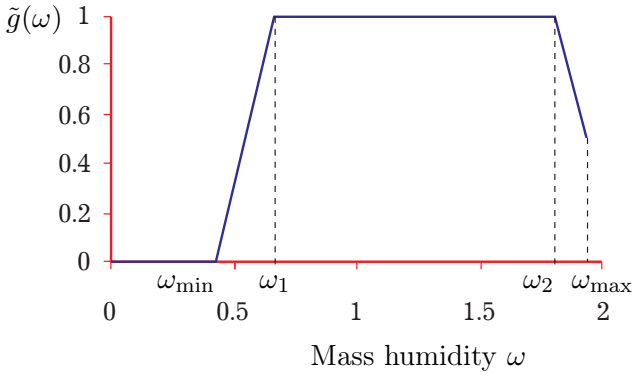

Fig. 2. The empirical function $\tilde{g}(\omega)$.

$$p_c(\theta_l) = p_{ce}\left(\frac{\theta_l}{\theta_s}\right)^{-b}, \qquad \theta_l(p_c) = \theta_s\left(\frac{p_c}{p_{ce}}\right)^{-\frac{1}{b}}, \tag{10}$$

$$k_{rl}(\theta_l) = \left(\frac{\theta_l}{\theta_s}\right)^{B} \quad \text{with} \quad B = 2b + 3,$$

$$k_{rb}(\theta_l) = \frac{\theta_l}{\theta_s}\left(1 - \frac{\theta_l}{\theta_s}\right)^2,$$

where θ_s is the saturation water content, p_{ce} is a scaling factor and b is a given parameter.

Changes of variables. In what follows we will introduce, instead of the pressures, the heights in column. These quantities are defined by:

$$h_l := \frac{p_l - p_0}{\rho_l g}, \tag{11}$$

$$h_b := \frac{p_b - p_0}{\rho_l g}, \tag{12}$$

$$h_c := h_b - h_l = \frac{p_c}{\rho_l g}, \tag{13}$$

where p_0 is the reference pressure, h_l (resp. h_b) represents the column height of leachate (resp. of biogas), and h_c the capillary height.

Taking into account these new variables, equations (8) and (9) become:

$$\mathbf{u}_l = -K\frac{k_{rl}(\theta_l)}{\mu_l}\rho_l g(\nabla h_l - \mathbf{e_z}), \tag{14}$$

$$\mathbf{u}_b = -K\frac{k_{rb}(\theta_l)}{\mu_b}\rho_l g\left(\nabla h_b - \frac{\rho_b}{\rho_l}\mathbf{e_z}\right). \tag{15}$$

In order to simplify the writing of these expressions, we note

$$k_l(\theta_l) := K\frac{k_{rl}(\theta_l)}{\mu_l}\rho_l g, \tag{16}$$

$$k_b(\theta_l) := K\frac{k_{rb}(\theta_l)}{\mu_b}\rho_l g, \tag{17}$$

k_l and k_b represent the hydraulic conductivity of leachate and biogas respectively.

Using (14) and (16) and taking into account that ρ_l is constant, equation (7) becomes:

$$\frac{\partial\theta_l}{\partial t} - \operatorname{div}(k_l(\theta_l)(\nabla h_l - \mathbf{e_z})) = \alpha_l\rho_l^{-1}. \tag{18}$$

Next, we have

$$\frac{\partial\theta_l}{\partial t} = \frac{d\theta_l}{dh_c}\frac{\partial h_c}{\partial t} = C_l(h_c)\frac{\partial h_c}{\partial t}, \tag{19}$$

where

$$C_l(h_c) = \frac{d\theta_l}{dh_c}$$

represents the capillary capacity. Using (13) and (16), the generalized Darcy flow of leachate (14) becomes

$$\mathbf{u}_l = k_l(\theta_l)(\nabla h_c - \nabla h_b + \mathbf{e_z}), \tag{20}$$

and from (18) and (19), we get

$$C_l(h_c)\frac{\partial h_c}{\partial t} - \operatorname{div}\left(k_l(\theta_l)(\nabla h_b - \nabla h_c - \mathbf{e_z})\right) = \alpha_l\rho_l^{-1}. \tag{21}$$

The continuity equation of the biogas phase is (with the notation (17))

$$\frac{\partial(\rho_b\theta_b)}{\partial t} - \operatorname{div}\left(\rho_b k_b(\theta_l)\left(\nabla h_b - \frac{\rho_b}{\rho_l}\mathbf{e_z}\right)\right) = \alpha_b, \tag{22}$$

which implies, since $\phi = \theta_l + \theta_b$,

$$(\phi - \theta_l)\frac{\partial\rho_b(h_b}{\partial t} + \rho_b(h_b)\frac{\partial(\phi - \theta_l)}{\partial t} - \operatorname{div}\left(\rho_b(h_b)k_b(\theta_l)\left(\nabla h_b - \frac{\rho_b}{\rho_l}\mathbf{e_z}\right)\right) = \alpha_b.$$

We assume that the compressibility of biogas obeys the ideal gas equation

$$\rho_b(h_b) = \rho_{0b}\left(\frac{p_b}{p_0}\right), \tag{23}$$

where p_0 and ρ_{0b} are respectively the pressure and the reference density.

Taking into account the relation (12), the equation (23) becomes

$$\rho_b = \rho_{0b}\left(1 + \frac{h_b}{h_0}\right),$$

where $h_0 = \frac{p_0}{\rho_l g}$, and this gives

$$(\phi - \theta_l)\frac{\rho_{0b}}{h_0}\frac{\partial h_b}{\partial t} - \rho_b(h_b)\frac{\partial \theta_l}{\partial t} - \operatorname{div}\left(\rho_b(h_b)k_b(\theta_l)\left(\nabla h_b - \frac{\rho_b}{\rho_l}\mathbf{e_z}\right)\right) = \alpha_b,$$

or

$$(\phi - \theta_l)\frac{\rho_{0b}}{h_0}\frac{\partial h_b}{\partial t} - \rho_b(h_b)C_l(h_c)\frac{\partial h_c}{\partial t} - \operatorname{div}\left(\rho_b(h_b)k_b(\theta_l)\left(\nabla h_b - \frac{\rho_b}{\rho_l}\mathbf{e_z}\right)\right) = \alpha_b.$$

We finally get the following system

$$\begin{cases} C_l(h_c)\dfrac{\partial h_c}{\partial t} + \operatorname{div}\,(\mathbf{u}_l) = \rho_l^{-1}\alpha_l, \\ \overline{k_l}(h_c)\mathbf{u}_l = \nabla h_c - \nabla h_b + \mathbf{e_z}, \\ A_1(h_c)\dfrac{\partial h_b}{\partial t} - A_2(h_c, h_b)\dfrac{\partial h_c}{\partial t} + \operatorname{div}(\rho_b(h_b)\mathbf{u}_b) = \alpha_b, \\ \overline{k_b}(h_c)\mathbf{u}_b = -\nabla h_b + c_1 h_b \mathbf{e_z} + c_2 \mathbf{e_z}, \end{cases} \tag{24}$$

which can also be written in the following form

$$\begin{cases} C_l(h_c)\dfrac{\partial h_c}{\partial t} - \operatorname{div}\left(k_l(\theta_l(h_c))(\nabla h_b - \nabla h_c - \mathbf{e_z})\right) = \alpha_l\rho_l^{-1}, \\ A_1(h_c)\dfrac{\partial h_b}{\partial t} - A_2(h_c, h_b)\dfrac{\partial h_c}{\partial t} - \operatorname{div}\left(\rho_b(h_b)k_b(\theta_l)\left(\nabla h_b - \dfrac{\rho_b(h_b)}{\rho_l}\mathbf{e_z}\right)\right) = \alpha_b, \end{cases} \tag{25}$$

where

$$\begin{aligned} A_1(h_c) &= \frac{(\phi - \theta_l(h_c))\rho_{0b}}{h_0}, \\ A_2(h_c, h_b) &= \rho_b(h_b)C_l(h_c), \\ \overline{k_l}(h_c) &= k_l(\theta_l(h_c))^{-1}, \\ \overline{k_b}(h_c) &= k_b(\theta_l(h_c))^{-1}, \\ c_1 = \frac{\rho_{0b}}{\rho_l h_0}, &\quad c_2 = \frac{\rho_{0b}}{\rho_l}, \end{aligned}$$

Boundary and initial conditions. To complete the equations of the compressible two-phase flow system (24), we consider the following boundary and initial conditions.

At $t = 0$, the initial conditions on the column heights in h_b and h_c are given by

$$h_c(0, x) = h_{c,0}(x), \quad x \in \Omega, \tag{26}$$

$$h_b(0, x) = h_{b,0}(x), \quad x \in \Omega. \tag{27}$$

We assume that, at the surface of the domain Γ_D, the contact with the atmosphere imposes Dirichlet-type conditions on the column heights of h_b and h_c. The limiting conditions on Γ_D are thus given by

$$h_c = h_{c,D} \quad \text{on} \quad \Gamma_D \times]0, T[, \tag{28}$$

$$h_b = h_{b,D} \quad \text{on} \quad \Gamma_D \times]0, T[. \tag{29}$$

We assume that the walls and the bottom of the domain are impermeable. These situations are represented by the following homogeneous Neumann conditions

$$k_l(\theta_l(h_c))(\nabla h_b - \nabla h_c - \mathbf{e_z}) \cdot \mathbf{n} = \mathbf{v}_l = 0 \quad \text{on} \quad \Gamma_N \times]0,T[, \tag{30}$$

$$k_b(\theta_l(h_c)) \left(\nabla h_b - \frac{\rho_b}{\rho_l} \mathbf{e_z} \right) \cdot \mathbf{n} = \mathbf{v}_b = 0 \quad \text{on} \quad \Gamma_N \times]0,T[. \tag{31}$$

Consequently, equations (25) together with boundary and initial conditions, give the following system

$$(S2) \begin{cases} C_l(h_c)\dfrac{\partial h_c}{\partial t} - \operatorname{div}(k_l(\theta_l(h_c))(\nabla h_b - \nabla h_c - \mathbf{e_z})) = \alpha_l \rho_l^{-1} & \text{in } \Omega \times]0,T[, \\ A_1(h_c)\dfrac{\partial h_b}{\partial t} - A_2(h_c,h_b)\dfrac{\partial h_c}{\partial t} - \operatorname{div}\left(\rho_b(h_b) k_b(\theta_l) \left(\nabla h_b - \dfrac{\rho_b(h_b)}{\rho_l} \mathbf{e_z} \right) \right) = \alpha_b & \text{in } \Omega \times]0,T[, \\ h_l = h_{l,D} \quad \text{and} \quad h_b = h_{b,D} & \text{on } \Gamma_D \times]0,T[, \\ k_l(\theta_l(h_c))(\nabla h_b - \nabla h_c - \mathbf{e_z}) \cdot \mathbf{n} = 0 \quad \text{and} \quad k_b(\theta_l(h_c)) \left(\nabla h_b - \frac{\rho_b}{\rho_l} \mathbf{e_z} \right) \cdot \mathbf{n} = 0 & \text{on } \Gamma_N \times]0,T[, \\ h_c(0,x) = h_{c,0}(x) \quad \text{and} \quad h_b(0,x) = h_{b,0}(x) & \text{in } \Omega. \end{cases} \tag{32}$$

2.3. The final model

The final mathematical model describing both the degradation of the organic mater and the compressible two-phase leachate-biogas during the anaerobic digestion process for biogas production is given by the system (2)=(S1) and the system (32)=(S2).

3. Variational formulation and semi-discrete system

In what follows, we make some assumptions.

Hypothesis 1. The coefficients α, K_d, Y, f_1 and f_2 fulfill the following conditions.

1. The proportion of nutrient recycling α cannot exceed 1
$$0 < \alpha \leqslant 1.$$
2. The mortality rate K_d is a positive parameter which is below the maximum growth rate
$$0 < K_d < \max_s \mu(s).$$
3. The rate of use of the substrate is a strictly positive parameter such that
$$0 < Y < 1.$$
4. The stoichiometric coefficients parameters f_1 and f_2 are strictly positive and satisfy
$$0 < f_1 < 1 \quad \text{and} \quad 0 < f_2 < 1.$$

The final model obtained in (2) and (32) is weakly coupled, therefore, we can separate the analysis of the system (2) and the system (32).

Due to the fact that the specific growth rate $\mu(\cdot)$ is a nonnegative and bounded function in both Monod and Haldane cases, and all the constants K_h, K_d, f_1, f_2 and Y lie in $]0,1[$, it is readily checked that assumptions of Theorem 1 in [43] are verified and we have the existence and the uniqueness of the solution of the system (2) (see [1]). We can also find a theorem of existence and uniqueness for the corresponding incompressible two-phase flow system in [36].

3.1. Semi-discretization in time and variational formulation of the system (S1)

Let $\tau_n = t^{n+1} - t^n$, $n = 0, \ldots, N$, where $N \in \mathbb{N}^*$, be a partition of $[0,T]$ with $t^0 = 0$ and $t^N = T$. In what follows we denote by f^n the values of a function f at the time t_n.

The semi-discrete scheme for the system (S1) considered here is the second order backward differentiation formula BDF2 for the variables (X,S,B) and the implicit Euler scheme for the ODE on

($[CO_2], [CH_4]$). The problem reads: find $\mathbf{U}^{n+1} \in Z = \left(H^1(\Omega)\right)^3$ such that

$$\int_\Omega \frac{3\mathbf{U}^{n+1} - 4\mathbf{U}^n + \mathbf{U}^{n-1}}{2\tau_n} \cdot \mathbf{v}\, dx + \int_\Omega \bar{\bar{D}} \nabla \mathbf{U}^{n+1} \cdot \nabla \mathbf{v}\, dx = \int_\Omega \mathbf{F^1}\left(\mathbf{U}^{n+1}\right) \cdot \mathbf{v}\, dx \qquad \forall \mathbf{v} \in Z, \tag{33}$$

where the initial values are computed as follow: find $\mathbf{U}^1 \in Z$ such that

$$\int_\Omega \frac{\mathbf{U}^1 - \mathbf{U}^0}{\tau_0} \cdot \mathbf{v}\, dx + \int_\Omega \bar{\bar{D}} \nabla \mathbf{U}^1 \cdot \nabla \mathbf{v}\, dx = \int_\Omega \mathbf{F^1}\left(\mathbf{U}^1\right) \cdot \mathbf{v}\, dx \qquad \forall \mathbf{v} \in Z, \tag{34}$$

and where the notation $\nabla \mathbf{U} \cdot \nabla \mathbf{v}$ means the vector with the components $\nabla U_i \cdot \nabla v_i$, for $i = 1, 2, 3$.

We linearize the scheme by using the Taylor formula

$$\mathbf{F^1}\left(\mathbf{U}^{n+1}\right) \simeq \mathbf{F^1}\left(\mathbf{U}^n\right) + J_{\mathbf{F^1}}\left(\mathbf{U}^n\right)\left(\mathbf{U}^{n+1} - \mathbf{U}^n\right), \tag{35}$$

where $J_{\mathbf{F^1}}$ is the Jacobian matrix of the vector function $\mathbf{F^1}$. Consequently, the final BDF2 scheme reads: find $\mathbf{U}^1 \in Z = \left(H^1(\Omega)\right)^3$ such that

$$\begin{aligned}\int_\Omega \left[\tau_0^{-1}\mathbf{I}_3 - J_{\mathbf{F^1}}\left(\mathbf{U}^0\right)\right] \mathbf{U}^1 \cdot \mathbf{v}\, dx + \int_\Omega \bar{\bar{D}} \nabla \mathbf{U}^1 \cdot \nabla \mathbf{v}\, dx \\ = \int_\Omega \left[\tau_0^{-1}\mathbf{U}^0 + \mathbf{F^1}\left(\mathbf{U}^0\right) - J_{\mathbf{F^1}}\left(\mathbf{U}^0\right)\mathbf{U}^0\right] \cdot \mathbf{v}\, dx \qquad \forall \mathbf{v} \in Z,\end{aligned} \tag{36}$$

and for all $n \geqslant 1$, find $\mathbf{U}^{n+1} \in Z$ such that

$$\begin{aligned}\int_\Omega \left[\frac{3}{2\tau_n}\mathbf{I}_3 - J_{\mathbf{F^1}}\left(\mathbf{U}^n\right)\right] \mathbf{U}^{n+1} \cdot \mathbf{v}\, dx + \int_\Omega \bar{\bar{D}} \nabla \mathbf{U}^{n+1} \cdot \nabla \mathbf{v}\, dx \\ = \int_\Omega \left[\frac{4\mathbf{U}^n - \mathbf{U}^{n-1}}{2\tau_n} + \mathbf{F^1}\left(\mathbf{U}^n\right) - J_{\mathbf{F^1}}\left(\mathbf{U}^n\right)\mathbf{U}^n\right] \cdot \mathbf{v}\, dx \qquad \forall \mathbf{v} \in Z.\end{aligned} \tag{37}$$

On the other hand, by using the Remark 1, the approximation of $\mathbf{G}$ at $t = t_{m+1}$ $\mathbf{G}^{m+1} = (u_4^{m+1}, u_5^{m+1})^T$, for $0 \leqslant m \leqslant n$, is given by

$$\frac{u_4^{m+1} - u_4^m}{\tau_m} = (1 - f_1)K_h u_1^{n+1} + (1 - f_2)\frac{1 - Y}{Y}\left(\frac{u_2^{m+1} - u_2^m}{\tau_m} + K_d u_2^{m+1}\right), \tag{38}$$

$$\frac{u_5^{m+1} - u_5^m}{\tau_m} = f_2\frac{1 - Y}{Y}\left(\frac{u_2^{m+1} - u_2^m}{\tau_m} + K_d u_2^{m+1}\right). \tag{39}$$

3.2. Semi-discretization in time and variational formulation of the system (S2)

The semi descretization in time and linearization of the flow sytem (S2) is realized in the implicit scheme and is written as follow

$$C_l(h_c^n)\frac{h_c^{n+1} - h_c^n}{\tau_n} - \operatorname{div}\left(k_l(h_c^n)(\nabla h_b^{n+1} - \nabla h_c^{n+1} - \mathbf{e_z})\right) = \rho_l^{-1}\alpha_l^{n+1} \qquad \text{in } \Omega, \tag{40}$$

$$\begin{aligned}A_1(h_c^n)\frac{h_b^{n+1} - h_b^n}{\tau_n} - A_2(h_c^n, h_b^n)\frac{h_c^{n+1} - h_c^n}{\tau_n} \\ - \operatorname{div}\left(\rho_b(h_b^n)k_b(h_c^n)\left(\nabla h_b^{n+1} - \frac{\rho_b(h_b^n)}{\rho_l}\mathbf{e_z}\right)\right) = \alpha_b^{n+1} \qquad \text{in } \Omega,\end{aligned} \tag{41}$$

where the unknowns h_c^{n+1} and h_b^{n+1} are the approximations of $h_c(t_{n+1})$ and $h_b(t_{n+1})$ such that the initial conditions are $h_c(0, x) = h_{c,0}(x)$ and $h_b(0, x) = h_{b,0}(x)$ in Ω and the boundary conditions are

$$h_c^{n+1} = h_{c,D} \quad \text{and} \quad h_b^{n+1} = h_{b,D} \quad \text{on} \quad \Gamma_D, \tag{42}$$

$$k_l(h_c^n)(\nabla h_b^{n+1} - \nabla h_c^{n+1} - \mathbf{e_z}) \cdot \mathbf{n} = 0 \quad \text{on} \quad \Gamma_N, \tag{43}$$

$$k_b(h_c^n)\left(\nabla h_b^{n+1} - \frac{\rho_b(h_b^n)}{\rho_l}\mathbf{e_z}\right) \cdot \mathbf{n} = 0 \quad \text{on} \quad \Gamma_N. \tag{44}$$

We introduce the following functional space

$$H_1 = \left\{ \mathbf{v} \in H^1(\Omega), \mathbf{v} = 0 \text{ on } \Gamma_D \right\}. \tag{45}$$

The weak formulation of (40)–(41) with the conditions (42)–(44) is written as follows:

$$\begin{cases} \text{Find } h_c^{n+1} \in h_{c,D} + H_1 \text{ and } h_b^{n+1} \in h_{b,D} + H_1 \text{ such that} \\ \displaystyle\int_\Omega C_l(h_c^n)\frac{h_c^{n+1}}{\tau_n}\psi\, dx + \int_\Omega k_l(h_c^n)(\nabla h_b^{n+1} - \nabla h_c^{n+1} - \mathbf{e_z})\cdot\nabla\psi\, dx \\ \qquad = \displaystyle\int_\Omega \rho^{-1}\alpha_l^{n+1}\psi\, dx + \int_\Omega C_l(h_c^n)\frac{h_c^n}{\tau_n}\psi\, dx, \quad \forall \psi \in H^1(\Omega) \\ \displaystyle\int_\Omega A_1(h_c^n)\frac{h_b^{n+1}}{\tau_n}\varphi\, dx - \int_\Omega A_2(h_c^n, h_b^n)\frac{h_c^{n+1}}{\tau_n}\varphi\, dx \\ \qquad + \displaystyle\int_\Omega \rho_b(h_b^n)k_b(h_c^n)\left(\nabla h_b^{n+1} - \frac{\rho_b(h_b^n)}{\rho_l}\mathbf{e_z}\right)\nabla\varphi\, dx = \int_\Omega \alpha_b^{n+1}\varphi\, dx \\ \qquad + \displaystyle\int_\Omega A_1(h_c^n)\frac{h_b^n}{\tau_n}\varphi\, dx + \int_\Omega A_2(h_c^n, h_b^n)\frac{h_c^n}{\tau_n}\varphi\, dx, \quad \forall \varphi \in H^1(\Omega) \end{cases} \tag{46}$$

4. Discrete problem

We assume in this section that Ω is a polygon domain of $\mathbb{R}^d$. Let $\mathcal{T}_h$ be a partition of $\bar{\Omega}$ into triangles T (in $\mathbb{R}^2$) or tetrahedra T (in $\mathbb{R}^3$) and we denote by $P_k(O)$ the space of polynomial functions defined in a subset O of $\mathbb{R}^d$ of total degree at most k. In order to define the full descretization of the problem (2),(32), we introduce the following finite-dimensional functional spaces:

$$Z_h = \left\{ \mathbf{v}_h \in \left(C(\bar{\Omega})\right)^3; \forall T \in \mathcal{T}_h\ \mathbf{v}_h|_T \in (P_1(T))^3 \right\}, \tag{47}$$

$$H_{0,h} = \left\{ \mathbf{v}_h \in C(\bar{\Omega}); \forall T \in \mathcal{T}_h\ \mathbf{v}_h|_T \in P_1(T) \right\}, \tag{48}$$

and

$$H_{1,h} = \left\{ \mathbf{v}_h \in C(\bar{\Omega}); \forall T \in \mathcal{T}_h\ \mathbf{v}_h|_T \in P_1(T),\ \mathbf{v}_h|_{\Gamma_D} = 0 \right\}. \tag{49}$$

4.1. Full discretization of the system (S1)

We discretize the equations (36)–(39) via the finite element method in the finite dimensional space Z_h. The problem consists to find $\mathbf{U}_h^1 \in Z_h$ such that

$$\begin{aligned} \int_\Omega \left[\tau_0^{-1}\mathbf{I}_3 - J_{\mathbf{F^1}}\left(\mathbf{U}^0\right)\right]\mathbf{U}_h^1\cdot\mathbf{v}\, dx + \int_\Omega \bar{\bar{D}}\nabla\mathbf{U}_h^1\cdot\nabla\mathbf{v}\, dx \\ = \int_\Omega \left[\tau_0^{-1}\mathbf{U}^0 + \mathbf{F^1}\left(\mathbf{U}^0\right) - J_{\mathbf{F^1}}\left(\mathbf{U}^0\right)\mathbf{U}^0\right]\cdot\mathbf{v}\, dx \qquad \forall \mathbf{v} \in Z_h, \end{aligned} \tag{50}$$

and for all $n \geqslant 1$, find $\mathbf{U}_h^{n+1} \in Z_h$ such that

$$\begin{aligned} \int_\Omega \left[\frac{3}{2\tau_n}\mathbf{I}_3 - J_{\mathbf{F^1}}\left(\mathbf{U}_h^n\right)\right]\mathbf{U}_h^{n+1}\cdot\mathbf{v}\, dx + \int_\Omega \bar{\bar{D}}\nabla\mathbf{U}_h^{n+1}\cdot\nabla\mathbf{v}\, dx \\ = \int_\Omega \left[\frac{4\mathbf{U}^n - \mathbf{U}^{n-1}}{2\tau_n} + \mathbf{F^1}\left(\mathbf{U}^n\right) - J_{\mathbf{F^1}}\left(\mathbf{U}^n\right)\mathbf{U}^n\right]\cdot\mathbf{v}\, dx \qquad \forall \mathbf{v} \in Z_h. \end{aligned} \tag{51}$$

On the other hand, we seek $\mathbf{G}_h^{m+1} = (u_{4h}^{m+1}, u_{5h}^{m+1})^T$, for $0 \leqslant m \leqslant n$, such that

$$\frac{u_{4h}^{m+1} - u_{4h}^{m}}{\tau_m} = (1-f_1)K_h u_{1h}^{n+1} + (1-f_2)\frac{1-Y}{Y}\left(\frac{u_{2h}^{m+1} - u_{2h}^{m}}{\tau_m} + K_d u_{2h}^{m+1}\right), \tag{52}$$

$$\frac{u_{5h}^{m+1} - u_{5h}^{m}}{\tau_m} = f_2\frac{1-Y}{Y}\left(\frac{u_{2h}^{m+1} - u_{2h}^{m}}{\tau_m} + K_d u_{2h}^{m+1}\right). \tag{53}$$

Remark 2. In our numerical simulations we choose $m = n$. Nevertheless, we write under this general form because it may be suitable for some applications to have two different time grids for the reaction-diffusion system and for the flow system.

4.2. Full discretization of the system (S2)

We discretize the equations (46) via the finite element method. The scheme consists to find $h_{ch}^{n+1} \in h_{c,D} + H_{1,h}$ and $h_{bh}^{n+1} \in h_{b,D} + H_{1,h}$ such that

$$\begin{cases} \displaystyle\int_\Omega C_l(h_{ch}^n)\frac{h_{ch}^{n+1}}{\tau_n}\psi\,dx + \int_\Omega k_l(h_{ch}^n)(\nabla h_{bh}^{n+1} - \nabla h_{ch}^{n+1} - \mathbf{e_z})\cdot\nabla\psi\,dx \\ \qquad = \displaystyle\int_\Omega \rho^{-1}\alpha_{lh}^{n+1}\psi\,dx + \int_\Omega C_l(h_{ch}^n)\frac{h_{ch}^n}{\tau_n}\psi\,dx, \quad \forall\psi \in H_{0,h}, \\ \displaystyle\int_\Omega A_1(h_{ch}^n)\frac{h_{bh}^{n+1}}{\tau_n}\varphi\,dx - \int_\Omega A_2(h_{ch}^n, h_{bh}^n)\frac{h_{ch}^{n+1}}{\tau_n}\varphi\,dx \\ \qquad\qquad + \displaystyle\int_\Omega \rho_b(h_{bh}^n)k_b(h_{ch}^n)\left(\nabla h_{bh}^{n+1} - \frac{\rho_b(h_{bh}^n)}{\rho_l}\mathbf{e_z}\right)\nabla\varphi\,dx \\ \qquad = \displaystyle\int_\Omega \alpha_{bh}^{n+1}\varphi\,dx + \int_\Omega A_1(h_{ch}^n)\frac{h_{bh}^n}{\tau_n}\varphi\,dx + \int_\Omega A_2(h_{ch}^n, h_{bh}^n)\frac{h_{ch}^n}{\tau_n}\varphi\,dx, \quad \forall\varphi \in H_{0,h}. \end{cases} \tag{54}$$

5. Numerical results

In this section we present some numerical results for the problem (2)–(32). In all the experiments, we take $\Omega \subset \mathbb{R}^n$, $\partial\Omega = \Gamma_D \cup \Gamma_N$, with $n = 2$ for the 2D case and $n = 3$ for the 3D case as follows:

- $L = 10\,\mathrm{m}$,
- for $n = 3$ (3D case), $\begin{cases} \Omega =]0, L[\times]0, L[\times]0, L[, \\ \Gamma_D = \{(x, y, 0), \text{ with } (x, y) \in]0, L[\times]0, L[\}, \end{cases}$
- for $n = 2$ (2D case), $\begin{cases} \Omega =]0, L[\times]0, L[, \\ \Gamma_D = \{(x, 0), \text{ with } x \in]0, L[.\} \end{cases}$

The different parameters used are given in Table 1 and Table 2 and come from [11] and [32]. From the same references, we take the initial conditions of the biodegradation system (in mgC/L) as indicated in Table 3.

The boundary conditions of the biodegradation system are all homogeneous Neumann conditions. The boundary and initial conditions for the flow system are given in Table 4.

We recall that at each time step, the system (2) is approximated by (50)–(53), and its solution gives the source terms of the two-phase flow system (32), approximated by (54). We note that some simulations of the 3D case are plotted with the software (Paraview) visualization tool.

Table 1. Parameters of the biodegradation.

K_H (d^{-1})	μ_m (d^{-1})	f_1	f_2	K_S (mgC/L)	K_d (d^{-1})	Y	α	K_I (mgC/L)
0.176	0.3	0.7	0.76	160	0.04	0.05	0.9	10

Table 2. Parameters of the porous medium.

θ_r	θ_s	K (m·s^{-1})	p_{ce} (m)	b	M_b (g/mol)	M_{H_2O} (g/mol)	A_m
0.27	0.9715	10^{-4}	-0.0323	2.5	30	18.01	0.8

μ_l (kg·m^{-1}·s^{-1})	μ_b (kg·m^{-1}·s^{-1})	C_{Tb} (m^3/kg)
$4.61027 \cdot 10^{-4}$	10^{-5}	0.178

Table 3. Initial conditions for the biodegradation system.

$X_0(x,y)$ (mgC/L)	$S_0(x,y)$ (mgC/L)	$[CO_2]_0(x,y)$ (mgC/L)	$[CH_4]_0(x,y)$ (mgC/L)
1751	0	0	0

Table 4. Initial and boundary conditions for the compressible two phase flow system.

$h_{c,0}(m)$ in Ω	$h_{b,0}(m)$ in Ω	$h_{c,D}(m)$ on Γ_D	$h_{b,D}(m)$ on Γ_D	$\mathbf{u}_l \cdot \mathbf{n}$ on Γ_N	$\mathbf{u}_b \cdot \mathbf{n}$ on Γ_N
$-1.3 \cdot 10^{-4}$	0	-0.0002	0	0	0

We recall that the landfill is considered to be an unsaturated and inhomogeneous porous medium due to a non-homogeneous distribution of the initial methanogenic bacteria B_0 as follows

— In 2D:

$$B_0(x,z) = \begin{cases} 1 & \text{in} \quad Z_1 := \{0 \leqslant x \leqslant L/2 \text{ and } 0 \leqslant z \leqslant L/2\}, \\ 2 & \text{in} \quad Z_2 := \{L/2 \leqslant x \leqslant L \text{ and } 0 \leqslant z \leqslant L/2\}, \\ 3 & \text{in} \quad Z_3 := \{0 \leqslant x \leqslant L \text{ and } L/2 < z < L\}. \end{cases}$$

— In 3D:

$$B_0(x,y,z) = \begin{cases} 1 & \text{in} \quad \sum_1 := \{0 \leqslant x \leqslant L/2, 0 \leqslant y \leqslant L \text{ and } 0 \leqslant z \leqslant L/2\}, \\ 2 & \text{in} \quad \sum_2 := \{L/2 \leqslant x \leqslant L, 0 \leqslant y \leqslant L \text{ and } 0 \leqslant z \leqslant L/2\}, \\ 3 & \text{in} \quad \sum_3 := \{0 \leqslant x \leqslant L, 0 < y < L \text{ and } L/2 \leqslant z < L\}. \end{cases}$$

We consider a quasi-uniform mesh of the domain Ω with (952 triangles and 517 vertices) in 2D and (48000 tetrahedrons and 9261 vertices) in 3D (see Fig. 3). We also consider $M_{bottom}(0.75L, 0.001L)$ a point at the bottom of the zone Z_3, in which we will observe the evolution of leachate stagnation.

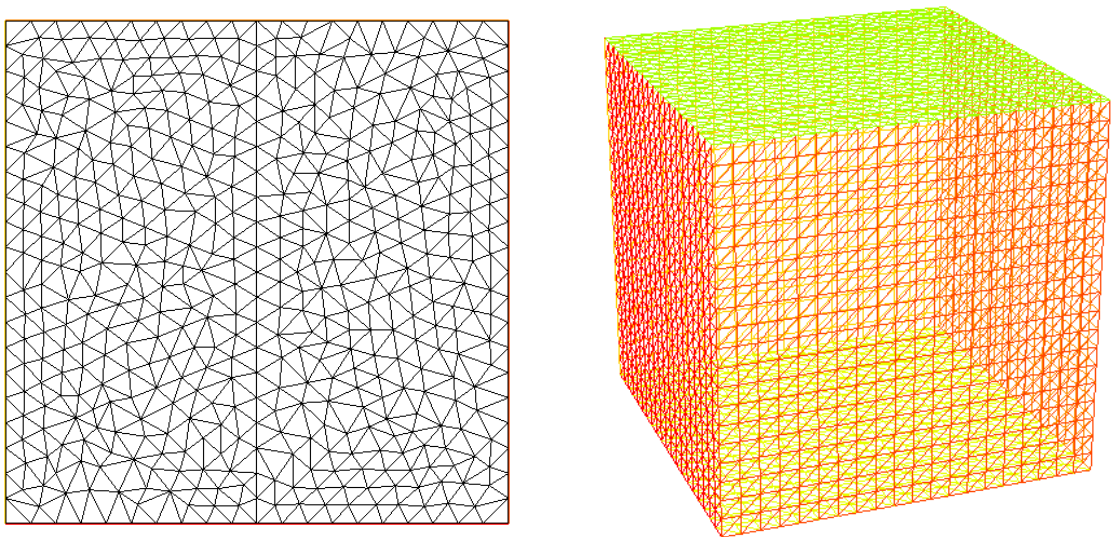

a (2D case) ***b*** (3D case)

Fig. 3. Mesh in 2D and 3D.

Taking into account the results obtained in [1] in terms of CPU computation time, we use partial (and not complete) diffusion. We then consider the diffusion $\bar{\bar{D}} = \{D_X = 0.01, D_S = 0.03, D_B = 0.05\}$ [m^2/d]. Using Haldane's law which is often more realistic, we obtain the following simulations.

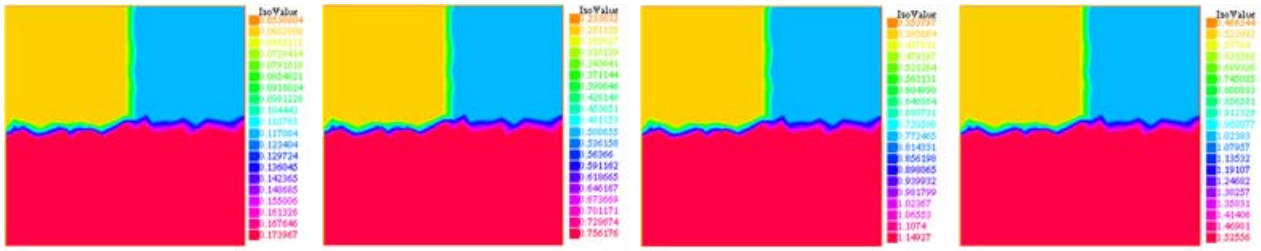

a $(t = 0.1$ day) ***b*** $(t = 0.5$ day) ***c*** $(t = 1$ day) ***d*** $(t = 1.8$ day)

Fig. 4. Evolution of methane production in 2D.

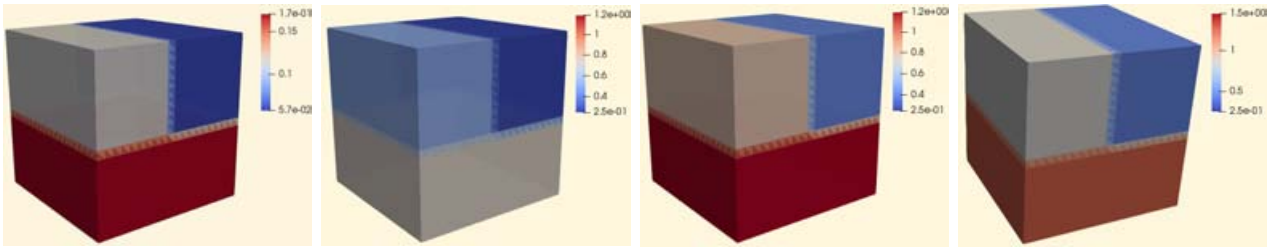

a $(t = 0.1$ day) ***b*** $(t = 0.5$ day) ***c*** $(t = 1$ day) ***d*** $(t = 1.8$ day)

Fig. 5. Evolution of methane production in 3D.

Figure 4 and Figure 5 show, respectively, the evolution of methane production in 2D and 3D at different times: $t_1 = 0.1$ day in (a), $t_2 = 0.5$ day in (b), $t_3 = 1$ day in (c) and $t_4 = 1.8$ day in (d).

From Figure 4, we notice that the the biogas production increases in the whole domain in proportion with the initial concentration of the methanogenic bacteria. More precisely, the mean value of the isovalues represented by "yellow color" goes from 0.06 at time t_1 to 0.52 at time t_4, for the "blue color" region it goes from 0.12 at time t_1 to 1.02 at time t_4, and the "red color" part from 0.17 at time t_1 to 1.52 at time t_4. This agree with the results reported in Figure 5. In Table 5, we summarize the intervals of the isovalues for each region.

Table 5. Table of the Max and Min values of the methane production isovalues in the three zones over time according to the solutions obtained in Figure 4.

Zones	t_1	t_2	t_3	t_4
$\sum_1$	Max = 0.09 Min = 0.05	Max = 0.39 Min = 0.23	Max = 0.60 Min = 0.35	Max = 0.80 Min = 0.46
$\sum_2$	Max = 0.13 Min = 0.10	Max = 0.56 Min = 0.42	Max = 0.85 Min = 0.64	Max = 1.13 Min = 0.85
$\sum_3$	Max = 0.17 Min = 0.14	Max = 0.75 Min = 0.59	Max = 1.15 Min = 0.89	Max = 1.52 Min = 1.19

Using the relationship between water content θ_l and capillary height h_c (see (10) and (13)), Figures 9 and 10 show the evolution of water content in 2D and 3D, respectively. Thus, we notice that the leachate starts to stagnate at the bottom of the domain at time t_4. More precisely, Figure 11 shows the evolution of the water content at the point M_{bottom} in two-phase biogas-leachate flow case and one phase leachate flow case (see [1]). We notice that the yellow curve "two-phase flow case" indicates the increase of the water content over time, from the initial value $\theta_0 = 0.37$, to the

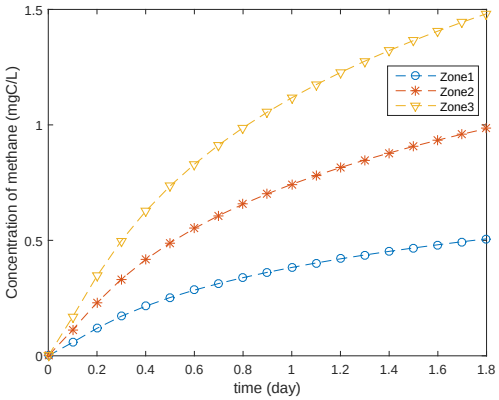

Fig. 6. Evolution of the average methane production in each zone $\sum_i$, $i \in \{1, 2, 3\}$ (zone 1 corresponds to $B_0 = 1$, zone 2 corresponds to $B_0 = 2$ and zone 3 corresponds to $B_0 = 3$).

value $\theta \approx \theta_s$ (value close to saturation), at time t_4. Almost, the same situation of the start of leachate stagnation was obtained at time $t = 2\,\text{day}$ in the case of single-phase leachate flow. Therefore, in the two-phase flow case and from the time t_4, we will not have the biogas production in the small layer at the bottom of the domain because its water content value does not satisfy the condition of humidity for the biogas production.

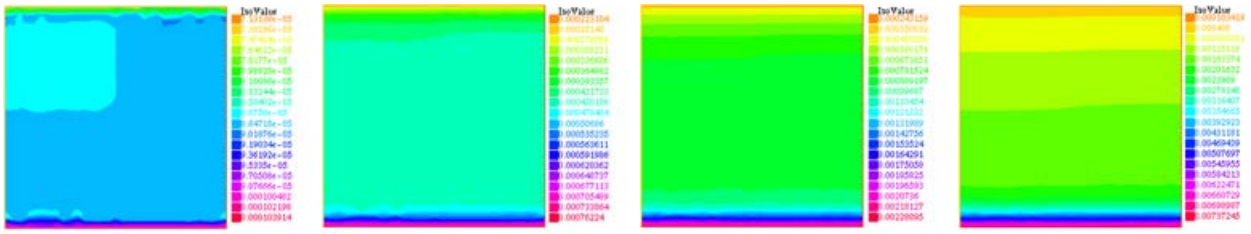

a $(t = 0.1\ \text{day})$ ***b*** $(t = 0.5\ \text{day})$ ***c*** $(t = 1\ \text{day})$ ***d*** $(t = 1.8\ \text{day})$

Fig. 7. Evolution of the column height of biogas h_b in 2D.

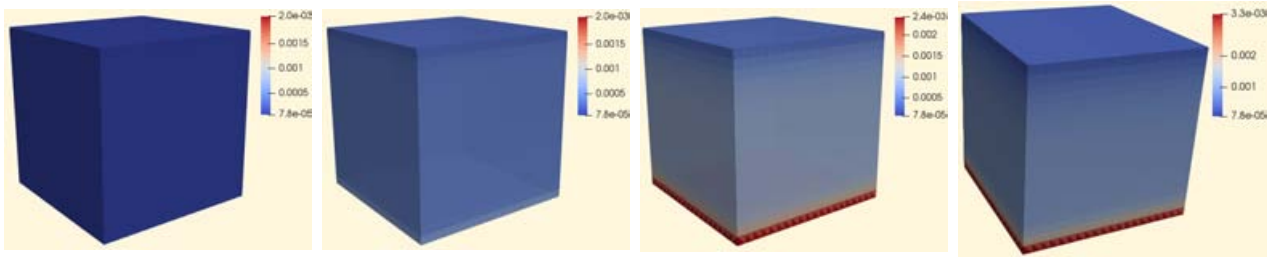

a $(t = 0.1\ \text{day})$ ***b*** $(t = 0.5\ \text{day})$ ***c*** $(t = 1\ \text{day})$ ***d*** $(t = 1.8\ \text{day})$

Fig. 8. Evolution of the column height of biogas h_b in 3D.

Figure 7 and Figure 8 show respectively the evolution of the column height of the biogas h_b in 2D and 3D. We notice in Figure 7*a*, which corresponds to time t_1, the appearance of a sky blue colored area with very low values and which almost coincides with the zone where initially the concentration of the methanogenic bacteria is the lowest. The diffusion process yields a monotonically increasing biogas production and the pressure distribution becomes regular and spatially homogeneous (see the figures (b), (c) and (d) in Figure 7).

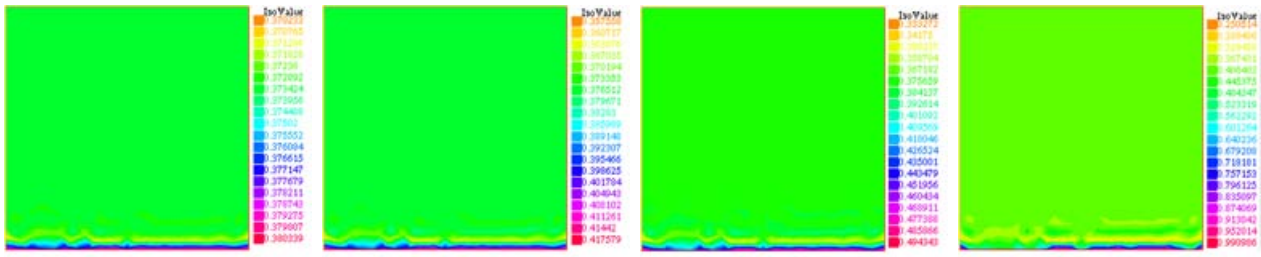

a $(t = 0.1\ \text{day})$ ***b*** $(t = 0.5\ \text{day})$ ***c*** $(t = 1\ \text{day})$ ***d*** $(t = 1.8\ \text{day})$

Fig. 9. Evolution of the water content $\theta(h_c)$ in 2D.

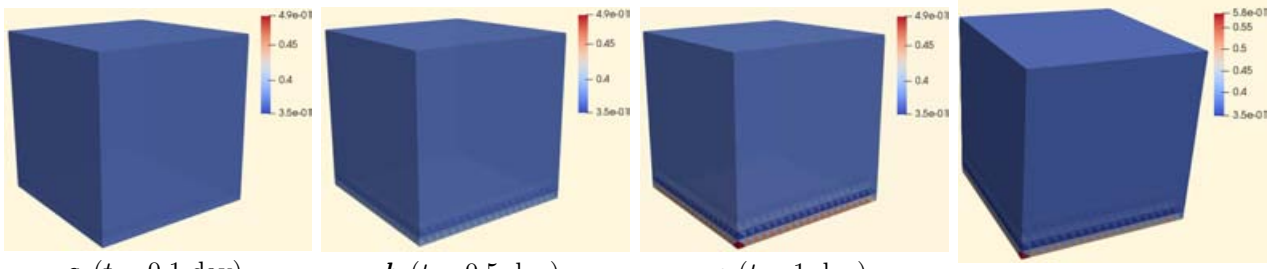

a $(t = 0.1\ \text{day})$ ***b*** $(t = 0.5\ \text{day})$ ***c*** $(t = 1\ \text{day})$ ***d*** $(t = 1.8\ \text{day})$

Fig. 10. Evolution of the water content $\theta(h_c)$ in 3D.

The time t_4 corresponds approximately to the moment when a leachate stagnation zone will appear at the bottom of the landfill. The moisture condition necessary for the biogas production will not be satisfied in the whole area after this time, this gives a stopping criterion for the algorithm. Accordingly, for the waste landfill management and the energy production, one has to decide either to release the stagnant leachate or to inject to act on the humidity factor which means mathematically to fit the proposed model in the framework of an optimal control approach.

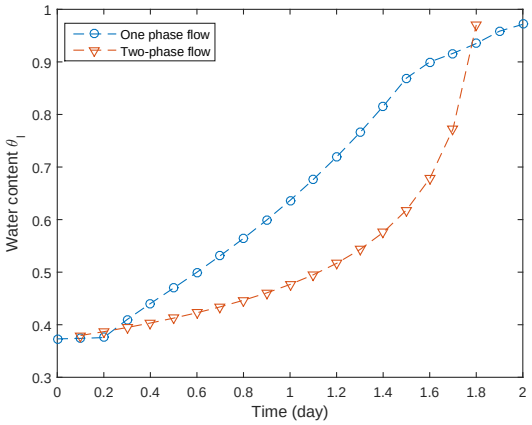

Fig. 11. Evolution of the water content θ_l at the point M_{bottom} in single-phase flow and two-phase flow problem.

6. Conclusion

In this article, we have considered a new model describing the bacterial activity in a household waste landfill taken as a reactive and unsaturated non-homogeneous porous medium. The coupling of the two-phase flow in the landfill and their interaction with the biological dynamics allows us to obtain accurately the leachate and the biogas. The outcome of the model, namely the pressure functions of these two phases, are the key variables for waste management and the energy production. The discrete setting which consists of a second-order BDF2 time-scheme and finite elements approximation give an efficient discrete framework with respect to the accuracy and reasonable cost requirements. The computation code in 2D and 3D and the numerical simulations confirm the relevance of the model and the associated discrete setting. Finally, we notice that the impact of the humidity on the outcome appears to be important and the combination of the approach developed in this article with an optimal control strategy can be a promising perspective.

Acknowledgments

The authors are gratefully for the French–Moroccan exchange program "PHC TOUBKAL 17/47".

[1] Belhachmi Z., Mghazli Z., Ouchtout S. Mathematical modeling and numerical approximation of a leachate flow in the anaerobic biodegradation of waste in a landfill. Mathematics and Computers in Simulation. **185**, 174–193 (2021).

[2] Hassam S., Ficara E., Leva A., Harmand J. A generic and systematic procedure to derive a simplified model from the anaerobic digestion model No. 1 (ADM1). Biochemical Engineering Journal. **99**, 193–203 (2015).

[3] Hénon F., Debenest G., Lefevre X., Pommier S., Chenu D., Quintard M. Simulation of Transport and Impact of Moisture Content on the Biodegradation. Fourth International Workshop "Hydro-Physico-Mechanics of Landfills". Santander, Spain (2011).

[4] Gallo C., Manzini G. A fully coupled numerical model for two-phase flow with contaminant transport and biodegradation kinetics. Communications in Numerical Methods in Engineering. **17** (5), 325–336 (2001).

[5] Chenu D. Modélisation des transferts réactifs de masse et de chaleur dans les installations de stockage de déchets ménagers: application aux installations de type bioréacteur. Doctoral dissertation, Institut National Polytechnique de Toulouse (2007).

[6] Ahusborde E., Amaziane B., El Ossmani M., Moulay M. Numerical Modeling and Simulation of Fully Coupled Processes of Reactive Multiphase Flow in Porous Media. J. Math. Study. **52** (4), 359–377 (2019).

[7] Pohland F. G., Al-Yousfi B. Design and Operation of Landfills for optimum stabilization and biogaz production. Water Science & Technology. **30** (12), 117–124 (1994).

[8] Harmand J., Lobry C., Rapaport A., Sari T. The Chemostat: Mathematical Theory of Microorganisms Cultures. ISTE Wiley (2017).

[9] Smith H. L., Waltman P. The theory of the chemostat: dynamics of microbial competition (Vol. 13). Cambridge University Press (1995).

[10] Dollé G., Duran O., Feyeux N., Frénod E., Giacomini M., Prud'Homme C. Mathematical modeling and numerical simulation of a bioreactor landfill using Feel++. ESAIM: Proceedings and Surveys. **55**, 83–110 (2016).

[11] Rouez M. Dégradation anaérobie de déchets solides: Caractérisation, facteurs d'influence et modélisations. Laboratoire de Génie Civil et d'Ingénierie Environnementale. Lyon, Institut National des Sciences Appliquées Docteur, 259 (2008).

[12] Fekih-Salem R., Harmand J., Lobry C., Rapaport A., Sari T. Extensions of the chemostat model with flocculation. Journal of Mathematical Analysis and Applications. **397** (1), 292–306 (2013).

[13] Rapaport A., Nidelet T., El Aida S., Harmand J. About biomass overyielding of mixed cultures in batch processes. Mathematical Biosciences. **322**, 108322 (2020).

[14] Rapaport A., Nidelet T., Harmand J. About biomass overyielding of mixed cultures in batch processes. 8th IFAC Conference on Foundations of Systems Biology in Engineering (FOSBE), Valencia, Spain, 15–18 Oct. (2019).

[15] Gnativ Z. Ya., Ivashchuk O. S., Hrynchuk Yu. M., Reutskyi V. V., Koval I. Z., Vashkurak Yu. Z. Modeling of internal diffusion mass transfer during filtration drying of capillary-porous material. Mathematical Modeling and Computing. **7** (2), 219–227 (2020).

[16] Dimitrova N., Krastanov M. Model-based optimization of biogas production in an anaerobic biodegradation process. Computers and Mathematics with Applications. **68** (9), 986–993 (2014).

[17] Bernard O., Hadj-Sadok Z., Dochain D., Genovesi A., Steyer J. P. Dynamical model development and parameter identification for an anaerobic wastewater treatment process. Biotechnology and Bioengineering. **75** (4), 424–438 (2001).

[18] Benyahia B., Sari T., Cherki B., Harmand J. Bifurcation and stability analysis of a two step model for monitoring anaerobic digestion processes. Journal of Process Control. **22** (6), 1008–1019 (2012).

[19] Didi I., Dib H., Cherki B. A Luenberger-type observer for the AM2 model. Journal of Process Control. **32**, 117–126 (2015).

[20] Arzate J. A., Kirstein M., Ertem F. C., Kielhorn E., Ramirez Malule H., Neubauer P., Cruz-Bournazou M. N., Junne S. Anaerobic digestion model (AM2) for the description of biogas processes at dynamic feedstock loading rates. Chemie Ingenieur Technik. **89**, 686–695 (2017).

[21] Hmissi M., Harmand J., Alcaraz-Gonzalez V., Shayeb H. Evaluation of alkalinity spatial distribution in an up-flow fixed bed anaerobic digester. Water Science and Technology. **77** (4), 948–959 (2018).

[22] Abaali M., Harmand J., Mghazli Z. Impact of Dual Substrate Limitation on Biodenitrification Modeling in Porous Media. Processes. **8** (8), 890 (2020).

[23] Pinder G. F., Gray W. G. Essentials of multiphase flow and transport in porous media. John Wiley and Sons (2008).

[24] Agostini F., Sundberg C., Navia R. Is biodegradable waste a porous environment? A review. Waste Management and Research. **30** (10), 1001–1015 (2012).

[25] Ouchtout S., Mghazli Z., Harmand J., Rapaport A., Belhachmi Z. Analysis of an anaerobic digestion model in landfill with mortality term. Communications on Pure and Applied Analysis. **19** (4), 2333–2346 (2020).

[26] Shi J., Wu Y., Zou X. Coexistence of Competing Species for Intermediate Dispersal Rates in a Reaction-Diffusion Chemostat Model. Journal of Dynamics and Differential Equations. **32** (2), 1085–1112 (2020).

[27] Nguyen-Ngoc D., Leye B., Monga O., Garnier P., Nunan N. Modeling microbial decomposition in real 3D soil structures using partial differential equations. International Journal of Geosciences. **4** (10A), 15–26 (2013).

[28] Vanrolleghem P. A., Dochain D. Dynamical Modelling and Estimation in Wastewater Treatment Processes. IWA Publishing (2001).

[29] Hecht F. New development in FreeFem++. Journal of numerical mathematics. **20** (3–4), 251–266 (2012).

[30] Lanini S. Analyse et modélisation des transferts de masse et de chaleur au sein des décharges d'ordures ménagères. Doctoral dissertation, Institut National Polytechnique de Toulouse (1998).

[31] Bellenfant G. Modélisation de la production de lixiviat en centre de stockage de déchets ménagers. Doctoral dissertation, Institut National Polytechnique de Lorraine-INPL (2001).

[32] Aran C. Modélisation des Ecoulements de Fluides et des Transferts de Chaleur au Sein des Déchets Ménagers. Application à la Réinjection de Lixiviat dans un Centre de Stockage. Ph.D. thesis, Institut National Polytechnique de Toulouse, France (2001).

[33] Helmig R. Multiphase flow and transport processes in the subsurface: a contribution to the modeling of hydrosystems. Springer-Verlag (1997).

[34] Chen Z., Huan G., Ma Y. Computational methods for multiphase flows in porous media (Vol. 2). Siam (2006).

[35] Kindlein J., Dinkler D., Ahrens H. Numerical modeling of multiphase flow and transport processes in landfills. Waste Management and Research. **24** (4), 376–387 (2006).

[36] Gabbouhy M., Mghazli Z. Un résultat d'existence de solution faible d'un système parabolique-elliptique non linéaire doublement dégénéré. Annales de la Faculté des sciences de Toulouse: Mathématiques. **10** (3), 533–546 (2001).

[37] Azaïez M., Deville M., Mund E. H. Éléments finis pour les fluides incompressibles. PPUR Presses polytechniques (2011).

[38] Lichtner P. C. Continuum formulation of multicomponent-multiphase reactive transport. Reviews in Mineralogy & Geochemistry. **34**, 1–82 (1996).

[39] Gholamifard S. Modélisation des écoulements diphasiques bioactifs dans les installations de stockage de déchets. Doctoral dissertation, Université Paris-Est (2009).

[40] Van Genuchten M. T. A closed-form equation for predicting the hydraulic conductivity of unsaturated soils. Soil Science Society of America Journal. **44** (5), 892–898 (1980).

[41] Campbell G. S. A simple method for determining unsaturated conductivity from moisture retention data. Soil Science. **117** (6), 311–314 (1974).

[42] Brooks R. H., Corey A. T. Hydraulic Properties of Porous Media. Colorado State Univ. Hydrology Paper No. 3 (1964).

[43] Bothe D., Fischer A., Pierre M., Rolland G. Global wellposedness for a class of reaction-advection-anisotropic-diffusion systems. Journal of Evolution Equations. **17** (1), 101–130 (2017).

Спряжений стисливий двофазний потік з біологічною динамікою, який моделює процес анаеробного біорозкладу відходів на сміттєзвалищі

Белхачмі З.[1,2], Мгазлі С.[3], Оухтаут З.[1,3]

[1] *Університет Верхнього Ельзасу, IRIMAS UR 7499, F-68100 Мюлуз, Франція*
[2] *Страсбурзький університет, Франція*
[3] *Університет Ібн Тофаїла, команда математичної інженерії (EIMA), лабораторія: ЕДП, алгебра та спектральна геометрія, Кенітра, Марокко*

У цій статті представлена та вивчається нова комбінована модель, яка поєднує біологічний та механічний аспекти, що описують відповідно процес виробництва біогазу та стисливий двофазний потік біогаз–фільтрат під час анаеробного біорозкладу органічних речовин на сміттєзвалищі, що розглядається як реактивне пористе середовище. Отримана модель описується реакційно-дифузійною системою бактеріальної активності у поєднанні зі стисливою двофазною системою потоку неоднорідного пористого середовища. Здійснено аналіз та чисельну апроксимацію моделі у межах варіаційного підходу. Запропоновано повну дискретну систему, засновану на часовій схемі BDF другого порядку та P1-сумісному скінченному елементі, та отримано ефективний алгоритм для спряженої системи. Виконано чисельне моделювання для 2D та 3D прикладів відповідно до теоретичного аналізу.

Ключові слова: *анаеробний біорозклад, стисливий двофазний потік, виробництво біогазу, спряжена модель, метод скінченних елементів.*